

Article

Biocompatibility and Antimicrobial Profile of Acid Usnic-Loaded Electrospun Recycled Polyethylene Terephthalate (PET)—Magnetite Nanofibers

Alexandra Elena Stoica (Oprea)¹, Alexandra Catalina Bîrcă¹, Dan Eduard Mihaiescu², Alexandru Mihai Grumezescu^{1,3,4}, Anton Ficăi^{1,4}, Hildegard Herman⁵, Baltă Cornel^{5,*}, Marcel Roșu⁵, Sami Gharbia⁵, Alina Maria Holban⁶, Bogdan Ștefan Vasile^{7,8}, Ecaterina Andronescu^{1,3} and Anca Oana Hermenean⁵

¹ Department of Science and Engineering of Oxide Materials and Nanomaterials, University Politehnica of Bucharest, 060042 Bucharest, Romania; oprea.elena19@gmail.com (A.E.S.); grumezescu@yahoo.com (A.M.G.); ecaterina.andronescu@upb.ro (E.A.)

² Department of Organic Chemistry, University Politehnica of Bucharest, 011061 Bucharest, Romania; danedmih@gmail.com

³ ICUB—Research Institute of the University of Bucharest, 060102 Bucharest, Romania

⁴ Academy of Romanian Scientists, Ilfov No. 3, 050044 Bucharest, Romania

⁵ Institute of Life Sciences, Vasile Goldis Western University of Arad, 310414 Arad, Romania; herman.hildegard@uvvg.ro (H.H.); samithgh2@hotmail.com (S.G.); hermenean.anca@uvvg.ro (A.O.H.)

⁶ Microbiology Immunology Department, Faculty of Biology, University of Bucharest, 030018 Bucharest, Romania; alina_m_h@yahoo.com

⁷ National Research Center for Micro and Nanomaterials, University Politehnica of Bucharest, 060042 Bucharest, Romania; bogdan.vasile@upb.ro

⁸ Research Center for Advanced Materials, Products and Processes, University Politehnica of Bucharest, 060042 Bucharest, Romania

* Correspondence: baltacornel@gmail.com or balta.cornel@uvvg.ro



Citation: Stoica, A.E.; Bîrcă, A.C.; Mihaiescu, D.E.; Grumezescu, A.M.; Ficăi, A.; Herman, H.; Cornel, B.; Roșu, M.; Gharbia, S.; Holban, A.M.; et al. Biocompatibility and Antimicrobial Profile of Acid Usnic-Loaded Electrospun Recycled Polyethylene Terephthalate (PET)—Magnetite Nanofibers. *Polymers* **2023**, *15*, 3282. <https://doi.org/10.3390/polym15153282>

Academic Editor: Ivan Gitsov

Received: 28 April 2023

Revised: 21 July 2023

Accepted: 26 July 2023

Published: 2 August 2023



Copyright: © 2023 by the authors. Licensee MDPI, Basel, Switzerland. This article is an open access article distributed under the terms and conditions of the Creative Commons Attribution (CC BY) license (<https://creativecommons.org/licenses/by/4.0/>).

Abstract: The highest amount of the world's polyethylene terephthalate (PET) is designated for fiber production (more than 60%) and food packaging (30%) and it is one of the major polluting polymers. Although there is a great interest in recycling PET-based materials, a large amount of unrecycled material is derived mostly from the food and textile industries. The aim of this study was to obtain and characterize nanostructured membranes with fibrillar consistency based on recycled PET and nanoparticles (Fe₃O₄@UA) using the electrospinning technique. The obtained fibers limit microbial colonization and the development of biofilms. Such fibers could significantly impact modern food packaging and the design of improved textile fibers with antimicrobial effects and good biocompatibility. In conclusion, this study suggests an alternative for PET recycling and further applies it in the development of antimicrobial biomaterials.

Keywords: recycled PET; magnetite; usnic acid; electrospinning; nanofibers; antimicrobial agents; in vitro; in vivo; biocompatibility

1. Introduction

Nanofibers have emerged as novel nanostructured materials with wide applicability [1] in numerous applications, including filtration [2], tissue engineering [3,4], biosensors [5,6], wound dressing [7,8], nanofibrous composites [9], protective clothing [10], food packaging [11], and drug delivery systems [12,13]. There are various techniques for nanofiber development, including electrospinning, phase separation, self-assembly, freeze-drying, template synthesis, the spinneret-based tunable engineered parameter method, and interfacial nanofiber polymerization [14]. Electrospinning (ES) represent a versatile and straightforward technique widely used to obtain continuous fibers from a large number of polymers, with diameters ranging from tens of nanometers to several micrometers [15,16].

The resulting fibrous mats have a large effective surface area, continuously interconnected pores (usually with high and controllable porosities) and high surface roughness [17].

Polyethylene terephthalate (PET) is a transparent and easy-to-process polymer, often utilized for food and beverage packaging [18]. Additionally, physico-chemical properties highlight PET as an ideal candidate for the design of shoes, clothing, bedding, and interior materials for automobiles [19]. Hence, there is a continuously increasing interest in the application of PET for medical purposes, such as artificial blood vessels, artificial heart valves, hernia repair meshes and scaffolds, and sewing rings [20–22].

As the third most commonly exploited polymer [13], the total global consumption of PET is around 13 million tons annually, mostly for fabricating packaging and textile fibers [23]. With an estimated production of 34 billion metric tons by 2050 [24], there is an increasing concern for the environment, which led many scientists to consider using recycled PET for different applications.

Nano-sized materials have superior physical and chemical properties compared to their bulk counterparts due to their mesoscopic, small object, quantum size, and surface effects [25,26]. Specifically, magnetite nanoparticles' characteristics, including non-toxicity, biocompatibility, and super-paramagnetism [27], make them ideal for biomedical application [28]. In this context, magnetite nanoparticles have been widely investigated in dynamic sealing [29], ecosystems [30], magnetic resonance imaging as contrast agents [31], therapeutic hyperthermia [32], biosensing [33,34], and magnetic targeted-drug delivery [35,36]. Moreover, magnetite nanoparticles have proved their efficiency in antimicrobial therapies due to their intrinsic antimicrobial properties and the capacity to deliver antimicrobial agents [37]. In this regard, nano-systems comprising magnetite nanoparticles functionalized with usnic acid, a lichen secondary metabolic compound with proven antimicrobial, antibiotic, and tissue regeneration capacities [38], represent a promising alternative for antimicrobial therapies. Moreover, recent studies have focused on incorporating magnetite-based bioactive materials containing antimicrobial agents or microorganism colonization inhibitors into nanostructured polymeric membranes. In recent decades, such approaches have significantly impacted their potential to overcome the challenges associated with biofilm formation and antimicrobial resistance.

This study aimed to develop and characterize nanostructured membranes with fibrillar consistency based on recycled PET and magnetite nanoparticles functionalized with usnic acid by electrospinning technique. To the best of our knowledge, no available studies report the direct synthesis of iron oxide nanoparticles onto the nanofibers' surface, as most use blends comprising PET and iron oxide nanoparticles for electrospinning. Moreover, the available studies do not investigate the biocompatibility or antimicrobial efficiency of the obtained biomaterials. Thus, we presumed to design a highly efficient antimicrobial biomaterial offering a potential alternative for recycling PET. The synthesized membranes' antimicrobial activity were assessed against *S. aureus*, *P. aeruginosa*, and *C. albicans*, in both planktonic and biofilm states, and the biocompatibility of the usnic acid-loaded electro-spun recycled PET nanofibers was assessed by in vitro and in vivo methods.

2. Materials and Methods

2.1. Materials

The polyester polymer was obtained from recycled PET coke bottles that were approved for the food industry. Dichloromethane ($M_w = 84.96$ g/mol) was acquired from Chimopar Trading SRL and trifluoroacetic acid ($M_w = 114.02$ g/mol) was purchased from Fluka Analytical. Ferrous sulfate 7-hydrate ($FeSO_4 \cdot 7H_2O$), ferric chloride ($FeCl_3$), and ammonia (NH_3 , 25%) were purchased from Sigma-Aldrich (St. Louis, MO, USA). All chemicals were of analytical purity and used with no further purification.

2.2. Electrospinning Deposition of PET Nanofibers

The electrospinning (ES) technique was utilized to fabricate nanostructured mats from recycled PET, according to our previously published article [39]. This method has been used

to obtain membranes consisting of fibrous networks with interconnected, overlapping, and randomly distributed fibers. First, the PET bottles were cut into small pieces (about 1 cm²) and then submerged in a mixture of dichloromethane and trifluoroacetic acid (volume ratio 1:8). The polymer was completely dissolved in the mixture, and electrospinning was performed using the parameters described in Table 1. The electrospinning procedure was carried out using a Tong Li Tech (Shenzhen, China) ES equipment, with a 23.26 kV voltage (−5.73 kV and 17.53 kV), 200 mm needle-to-target distance, and 5, 7.5 and 10 mL/h, respectively, flow rate for 30 min for all solutions.

Table 1. The parameters used for electrospinning.

Sample	Output 1 (kV)	Output 2 (kV)	Heat (kW)	Humidity (%)	Temperature (°C)	Feed Rate (mL/h)
PET_5_ctrl						5
PET_7.5_ctrl	−5.73	17.53	0.6	35	27	7.5
PET_10_ctrl						10

2.3. Magnetite (Fe₃O₄) Functionalized with Usnic Acid (UA) Synthesis

The iron oxide nanoparticles were obtained by wet chemical precipitation from aqueous iron salt solutions using alkaline media.

The usnic acid-functionalized magnetic nanoparticles were prepared using wet chemical co-precipitation from aqueous iron salt solutions using alkaline media. Thus, a first solution of Fe²⁺ and Fe³⁺ in 1:2 molar ratio was prepared (300 mL) according to Refs. [40–42]. Then, a second solution was made using NH₄OH solution (25%, 9 mL) and added to a 0.03% solution of usnic acid (300 mL).

2.4. Polyethylene Terephthalate (PET)—Magnetite Nanofibers Functionalized with Usnic Acid Synthesis

PET nanofibers obtained via electrospinning were cut into 1 cm² pieces and submerged in the first solution for 10 min (described in Section 2.3). After that, they were submerged in the second solution for another 10 min (described in Section 2.3). Subsequently, the samples were washed with distilled water and left to dry at room temperature overnight. Thus, depending on the feed rate of the electrospinning, three types of samples were obtained and noted accordingly (PET@Fe₃O₄@UA_5, PET@Fe₃O₄@UA_7.5, and PET@Fe₃O₄@UA_10).

2.5. Physico-Chemical Characterization

2.5.1. Fourier-Transform Infrared Spectroscopy

IR spectra were obtained with a Nicolet iN10 MX Fourier-transform (FT-IR) microscope from Thermo Fischer Scientific (Waltham, MA, USA) equipped with a liquid nitrogen-cooled mercury cadmium telluride (MCT) detector. The spectral collection was registered in reflection mode at a resolution of 4 cm^{−1} in the 700–4000 cm^{−1} wavenumber range, and 32 scans were co-added for each spectrum and converted to absorbance using the OmnicPicta software (version 8.2 Thermo Nicolet) from Thermo Scientific.

2.5.2. X-ray Diffraction (XRD)

Grazing incidence X-ray Diffraction (GIXRD) was investigated with a PANalytical Empyrean diffractometer (PANalytical, Almelo, The Netherlands) utilizing CuK radiation (=1.541874 Å) equipped with a 2 × Ge (2 2 0) hybrid monochromator for Cu and a parallel plate collimator on the PIXcel3D. With a step size of 0.04° and a time for each step of 3 s, scanning was carried out on the 2θ axis in the range of 5–80° with an incidence angle of 0.5°.

2.5.3. Scanning Electron Microscopy

The morphology and size of the fiber mats were carried out by Scanning Electron Microscopy using equipment purchased from FEI (Hillsboro, OR, USA). The samples were

cut with a diamond disc and fixed on a sample support for placement in the analysis chamber. The obtained images are obtained by recording the resultant secondary electron beam with 30 keV energy at different points of the samples.

2.5.4. Transmission Electron Microscopy

In order to obtain important information on the inmate microstructure of fibrous mats, Transmission Electron Microscopy (TEM) images were acquired. The samples were fixed on a carbon-coated copper grid at room temperature (RT). Obtaining TEM images was possible by analyzing the sample using a high-resolution Tecnai™ G2 F30 S-TWIN transmission microscope equipped with SAED, purchased from Thermo Fisher Scientific (former FEI, Hillsboro, OR, USA). This equipment operates in transmission mode using 300 kV voltage, the point and line resolution guaranteed, with values of 2 Å and 1 Å, respectively.)

2.5.5. FT-ICR-MALDI

The FT-ICR MALDI method involves positive ionization mode, 4 M data acquisition magnitude, 90–2500 uam mass range, 100 V plate offset voltage, 260 V deflector plate voltage, 25% laser power with 250 laser shots at 1500 Hz frequency and, for ion optics, 0.7 ms time of flight at 4 Mhz frequency, 350 Vpp RF amplitude.

2.6. Biological Characterization

2.6.1. In Vitro Antibacterial Experiments

Growth of planktonic (free-floating) microorganisms in the presence of materials. To test the effect on planktonic microorganism growth, the obtained materials were cut into 1 cm/1 cm samples and then sterilized by exposure to UV radiation for 30 min on each side. One fragment of sterile material was individually deposited in a well of a sterile 6-well plate, 2 mL of nutritive broth was added to each well, and then 20 µL of 0.5 McFarland microbial suspension (*Staphylococcus Aureus* ATCC 23235 and *Pseudomonas aeruginosa* ATCC 25619) or 1 McFarland (yeast—*Candida albicans*) prepared in sterile physiological water (0.9% NaCl solution). The 6-well plates were incubated at 37 °C for 24 h. After the incubation time expiration, 200 µL of the obtained microbial suspensions were transferred to 96 sterile plates, and the turbidity of the microbial cultures (absorbance) was measured spectrophotometrically at 600 nm.

Evaluation of adhesion and biofilm formation. To test the effect of fibrillated materials on adhesion and biofilm production, the materials were cut to 1 cm/1 cm and sterilized by exposure to UV radiation for 20 min on each side. One fragment of sterile material was individually deposited in a well of a 6-well sterile plate, and 2 mL of liquid medium and then 20 µL of 0.5 McFarland (bacteria—*S. aureus* and *P. aeruginosa*) or 1 McFarland (yeast—*C. albicans*) microbial suspension prepared in sterile physiological water were added to the wells. The plates were incubated at 37 °C for 24 h. After incubation, the materials were washed with sterile saline water and placed into the sterile nutritive broth. The samples were incubated for different periods (24, 48, and 72 h, respectively) to allow the development of attached cells and biofilm formation. After the expiration of each incubation period, the sample on which the biofilm was developed was washed with sterile saline water and placed in 1 mL of sterile saline water. The tube was vigorously vortexed for 30 s and sonicated for 10 s to separate the cells from the biofilm. The prepared cell suspension was diluted, and different dilutions were seeded on solid culture media plates to result in and quantify colony-forming units (CFU/mL). The statistical significance (* $p \leq 0.05$, ** $p < 0.001$) was determined using the non-parametric two-way ANOVA algorithm Bonferroni test.

2.6.2. In Vivo Experiments

Animals and experimental design. The in vivo experiments were performed after the approval of the protocol by the Research Ethics Commission of the Vasile Goldis Western University of Arad.

Experimental studies used adult CD1 mice housed in IVC cages with standard breeding conditions in the university's animal facility.

The materials sterilized in UV light (30 min on each side) were implanted in a subcutaneous pocket in the dorsal region, under anesthesia, by intraperitoneal administration of xylazine/ketamine.

Seven experimental groups ($n = 10$) were performed, as follows: control, PET_5_ctrl, PET_7.5_ctrl, PET_10_ctrl, PET@Fe₃O₄@UA_5, PET@Fe₃O₄@UA_7.5, and PET@Fe₃O₄@UA_10, and euthanized after 24 h and 7 days after surgery.

After the surgery, the animals were housed individually and examined clinically every day by a vet, according to the following parameters: the appearance of surgery, redness, infection, edema/abscess, hematoma, and scars. Biopsies were performed 24 h, respectively, 7 days after implantation, under anesthesia. Blood was also collected by cardiac puncture for biochemical analysis.

Biochemistry. The collected blood was centrifuged at 3500 rpm for 10 min. Samples were analyzed for C-reactive protein (CRP) level evaluation on a Mindray BS-120 (Shenzhen-Mindray Bio-Medical Electronics Co., Ltd., Nanshan, Shenzhen, China) chemistry analyzer, using the CRP FL reagent kit (ChemaDiagnostica, Monsano, Italy).

Histology. The surrounding tissue's implant area was fixed in 4% paraformaldehyde solution, embedded in paraffin, sectioned at 5 μ m, and stained with hematoxylin and eosin (H&E) and Masson Goldner trichrome. The microscopic sections were analyzed under the microscope (Olympus BX43 equipped with an Olympus XC30 digital camera and CellSens software V4.2, Shinjuku, Japan). Sections were scored to grade the inflammation, fibrosis, and neovascularization. Each histometric parameter was graded on a scale of 0–4 for the amount of tissue reaction: – (not present) to ++++ (extensive).

Immunofluorescence. Deparaffinization and rehydrated sections were exposed to primary antibody TNF- α (Abcam (Cambridge, UK), dilution 1:100) after antigen unmasking with sodium citrate buffer (pH 6.0) and BSA blocking for 1 h. Alexa Fluor dye conjugated (1:500) was used as a secondary antibody, and nuclei were counterstained with DAPI. The fluorescence was visualized by confocal microscopy (Leica TCS SP8 confocal microscope, Wetzlar, Germany).

3. Results and Discussions

The nanostructured membranes obtained by electrospinning and subsequently impregnated with magnetite nanoparticles functionalized with usnic acid have been characterized by FT-IR, XRD, SEM and TEM. Fe₃O₄@UA characterization has been presented elsewhere [41]. Furthermore, previous attempts have been made to develop magnetic nanofibers based on iron oxide nanoparticles and PET through the electrospinning method [43,44]. However, to the best of our knowledge, no available studies report the direct synthesis of iron oxide nanoparticles onto the nanofibers' surface, as most use blends comprising PET and iron oxide nanoparticles for electrospinning. Moreover, the available studies do not investigate the biocompatibility or antimicrobial efficiency of the obtained biomaterials.

3.1. X-ray Diffraction

Figure 1 shows the X-ray diffractogram recorded for PET@Fe₃O₄@UA. A single crystalline phase along with the diffractive interference characteristic of the magnetite is observed. However, the presence of PET resulted in a reduced crystallinity of the sample. The planes (220), (311), (400), (422), (511), (440) and (533) Bragg's reflections attributed to 2θ angle: 30.2°, 35.6°, 43.2°, 53.7°, 57.2°, 62.8° and 74.3° correspond to the face-centered cubic (fcc) structures of magnetite, which are in accordance with JCPDS No. 79-0417 [45,46].

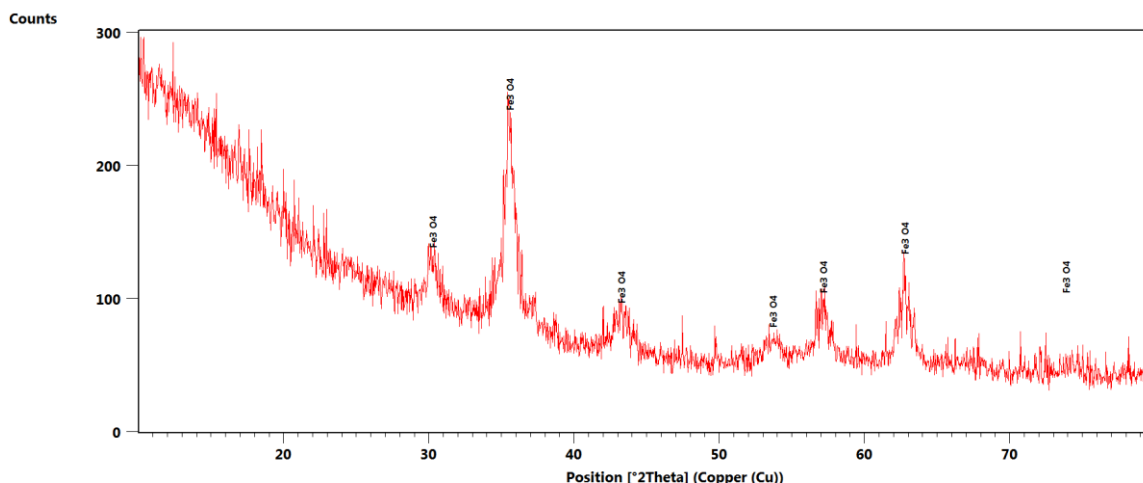


Figure 1. X-ray diffractogram recorded for PET@Fe₃O₄@UA.

3.2. Scanning Electron Microscopy

Scanning Electron Microscopy (SEM) was used to characterize the morphology of the nanostructured membranes obtained via electrospinning at various feed rates and to confirm the nanoparticles' presence on the surface of the nanofibers. The results are shown in Figure 2. A nanostructured wire network with diameters ranging from 50 to 150 nm is observed for all experimental deposition rates. Furthermore, it can be seen that Fe₃O₄@UA are randomly distributed, usually at the junction of the fibers, which act as nucleation centers favoring the growth of magnetite nanocrystals. While the size of the nanofibers is smaller, the distribution of the nanoparticles is in accordance with our previous work [39]. Furthermore, the particle size present on the surface of the junction between the fibers varies between 5 and 10 nm.

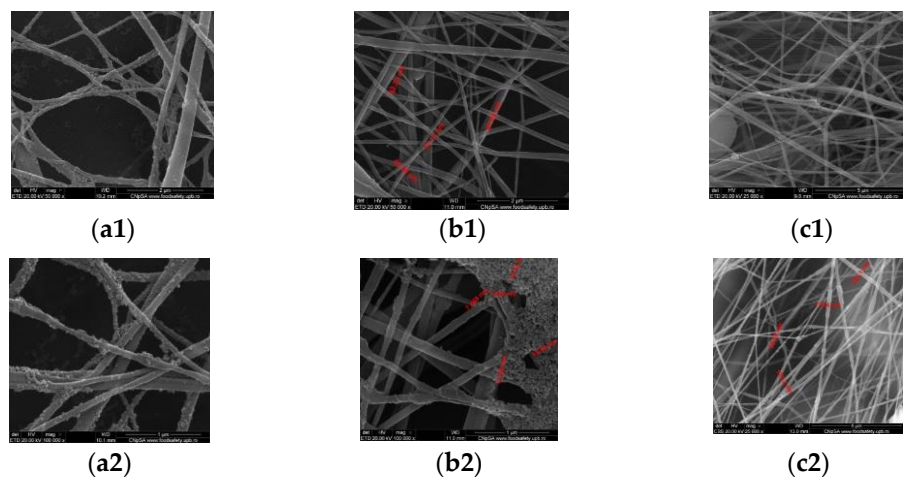


Figure 2. SEM images for PET@Fe₃O₄@UA at various flows ((a1,a2)—5 mL/h; (b1,b2)—7.5 mL/h; (c1,c2)—10 mL/h).

Therefore, it can be assumed that the formation of nanoparticles directly onto the nanofibers' surface does not affect their size, morphology, and properties. However, the tendency of the magnetite nanoparticles to form clusters at the nanofibers' junction could further affect their antimicrobial potency due to a consequently reduced bioavailability [47] and to their mechanical properties [48]. The nanoparticle aggregation issue could be resolved by subjecting the solutions in which the PET meshes are immersed to magnetic stirring, thus ensuring a homogenous deposition of the iron precursors onto the nanofibers' surface.

3.3. Transmission Electron Microscopy

TEM characterization further confirmed the results obtained through SEM analysis. TEM images are shown in Figure 3. Thus, the nanometric diameter of the fibers with sizes between 50 and 150 nm is confirmed, with a non-homogenous distribution of the nanoparticles onto their surface. Results from previous studies focusing on the development of PET nanofibers through the electrospinning method report significantly higher nanofiber sizes [49,50].

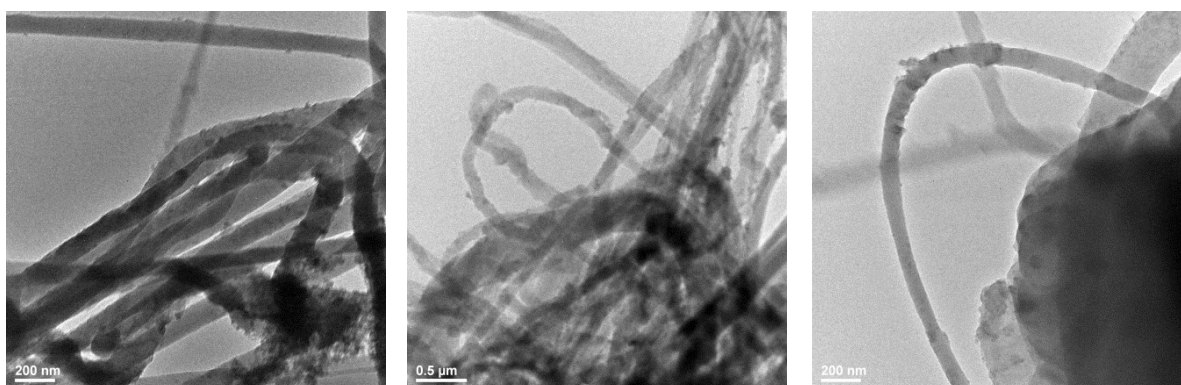


Figure 3. TEM images for nanostructured membranes of PET@Fe₃O₄@UA at a flow rate of 5 mL/h (PET@Fe₃O₄@UA_5).

3.4. Fourier-Transform Infrared Spectroscopy

FT-IR was used to assess the integrity of functional groups after the electrospinning process. The results obtained are shown in Figure 4 and highlight the presence of PET-absorbing bands, namely 1712 cm⁻¹ and 1240 cm⁻¹, characteristic for the C=O of the ester group and absorption bands for the asymmetrical C-O-C stretching and C-H aromatic ring bonds at 1093 cm⁻¹ and 722 cm⁻¹, respectively [51–53]. Additionally, the absorption band at 1017 cm⁻¹ is characteristic of the in-plane vibration of benzene [54]. No movement of the absorption bands is observed. The Fe-O bond absorption band characteristic for magnetite is not observed. The amount of magnetite nanoparticles was under the detection limit of diamond-ATR crystal.

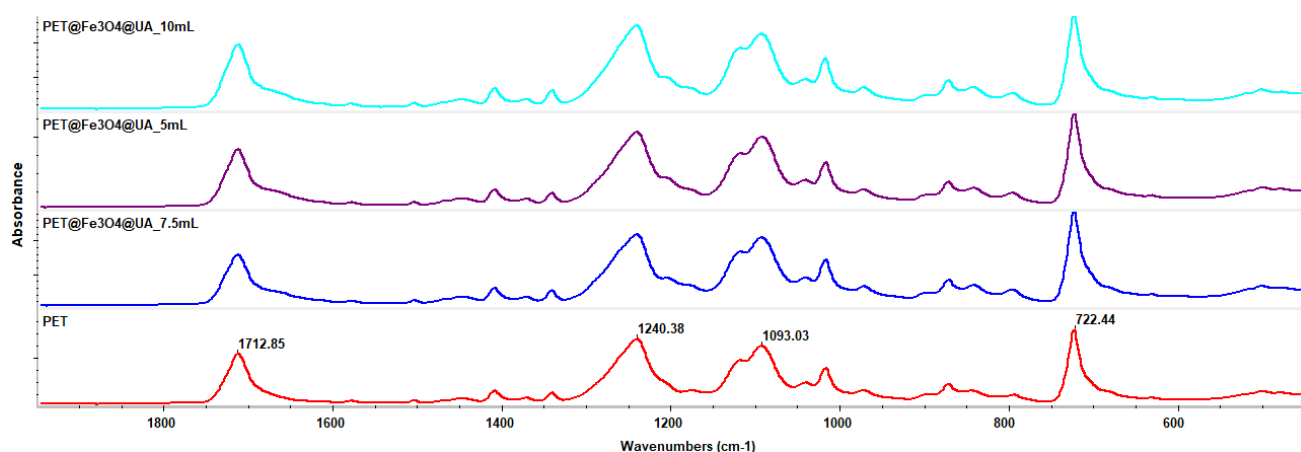


Figure 4. The FT-IR spectra for PET@Fe₃O₄@UA membranes.

3.5. FT-ICR MALDI

The usnic acid identification was performed by HR-FT-ICR-MS method using the MALDI sample introduction technique and DHB (di-hydroxybenzoic acid) matrix. As a mass reference compound, high-purity usnic acid was used (middle spectrum in figure—green) and the mass confirmation was performed by Compass DataAnalysis mass cluster

simulator (black spectrum, down). The sample mass peak (red spectrum, upside) proves a low mass difference from the usnic acid reference at a 288,625 FWHM mass resolution, allowing a positive identification of usnic acid in the thin film sample (Figure 5). The sample preparation method involves sample and usnic acid reference immobilization on an ITO-grafted slide and DHB matrix (methanolic solution) deposition (nebulization) before FT-ICR analysis (Figure 6).

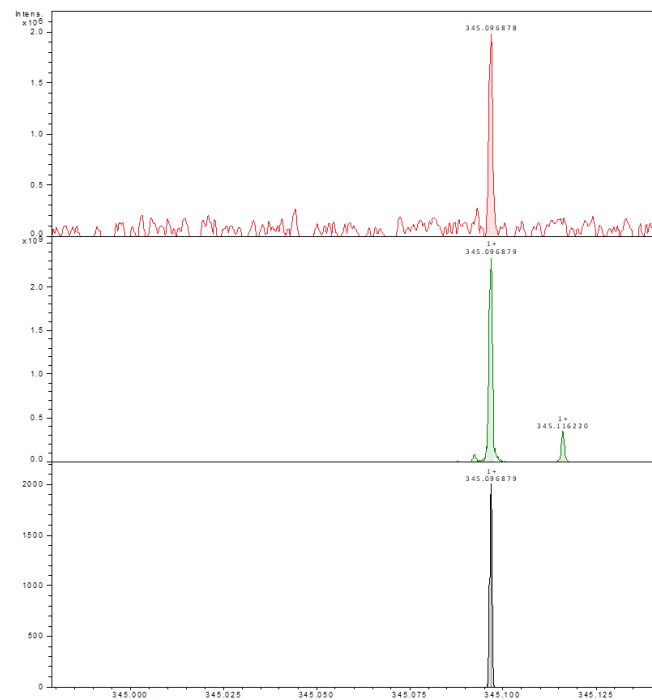


Figure 5. Zoom-in from the full spectrum (upside) to the monoisotopic peak of usnic acid, sample (red), reference (green), and simulated spectrum (black).

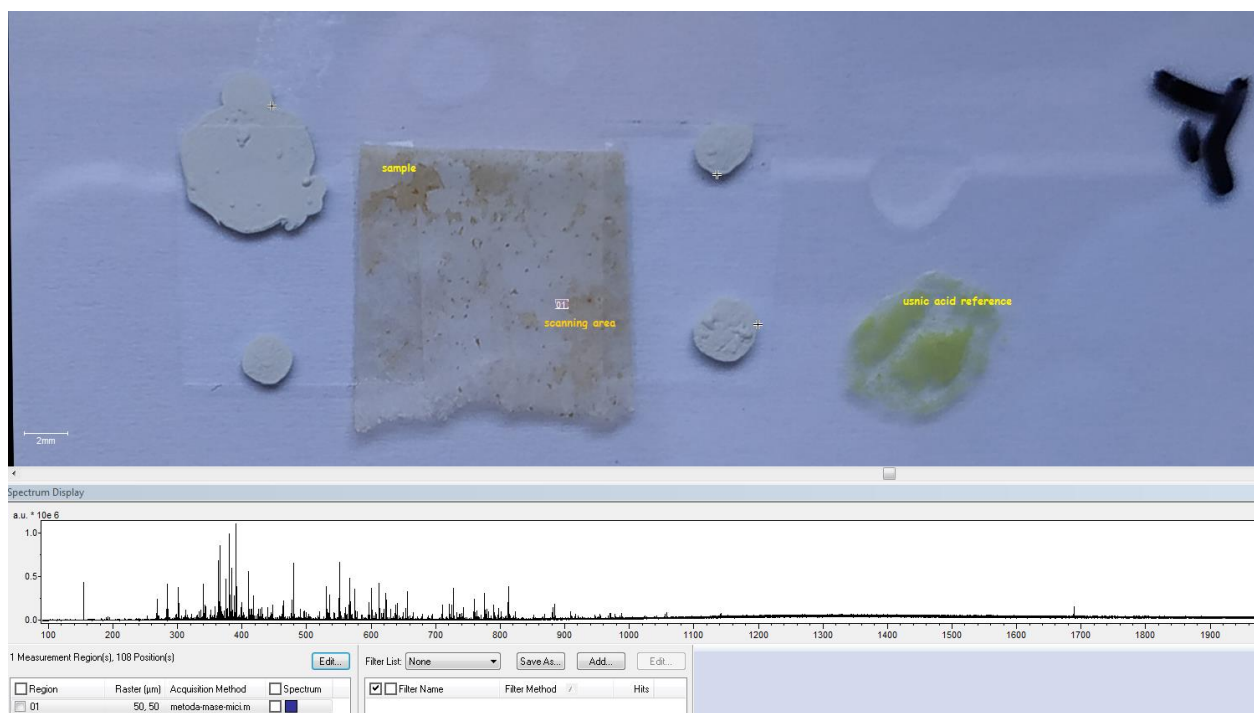


Figure 6. MALDI slide, sample (PET@Fe₃O₄@UA), reference compound, and scanning area.

A further surface scan of the sample (108 data acquisition points, $50 \times 50 \mu\text{m}$ spacing) reveals a relative homogeneous surface distribution of usnic acid in the scanned area (Figures 7 and 8).

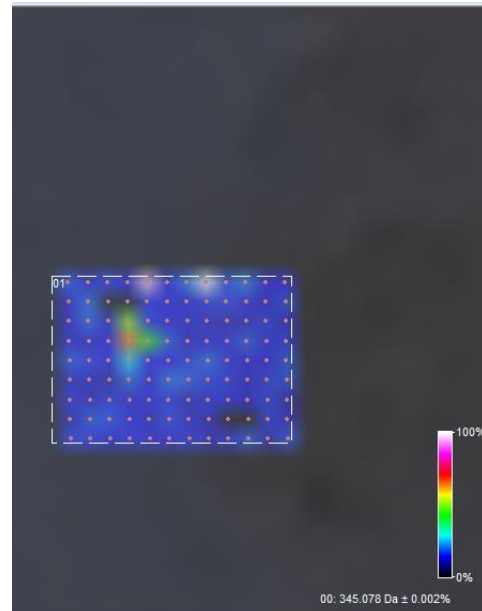


Figure 7. Surface distribution of usnic acid M+H peak, C₁₈H₁₆O₇.

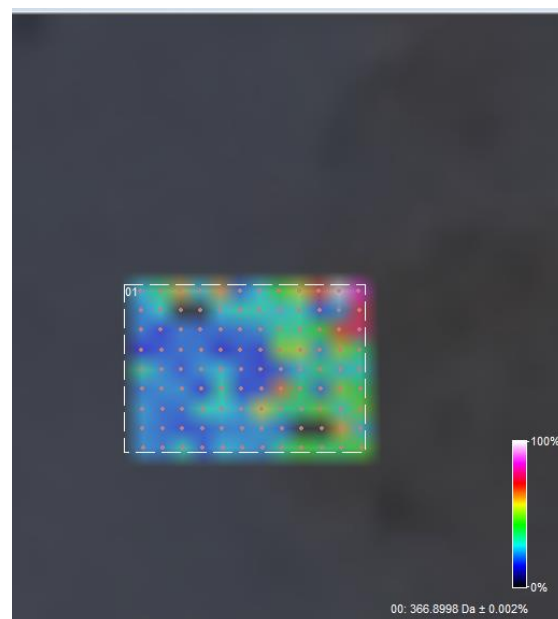


Figure 8. Surface distribution of usnic acid M+Na peak, C₁₈H₁₆O₇Na.

3.6. *In Vitro* Biocompatibility

Antimicrobial Effect

Contamination of foods and medical surfaces with pathogenic microorganisms represents a significant risk factor for consumers and patients. Microorganisms can grow both in free-floating (planktonic) cultures and attached to surfaces by producing highly specialized multicellular communities called biofilms. Adherent microorganisms have different biochemical and genetic traits and represent an additional risk factor, as they are more difficult to remove and more resistant than microorganisms that develop in a planktonic state. Biofilm bacteria show behavior-related resistance to antimicrobials and

host defense mechanisms, which differs from genetically acquired microbial resistance, and is known as tolerance. In this context, alternative methods for limiting microbial colonization and biofilm formation are being intensively studied for industrial and medical purposes [55,56].

For *S. aureus* planktonic cultures (Figure 9), it was observed that recycled PET containing $\text{Fe}_3\text{O}_4@UA$ nanoparticles had a significant inhibitory effect against microbial growth. It can be observed that the highest inhibitory activities were achieved in PET samples at which the fibers deposition by electrospinning was realized at a flow rate of 10 mL/h, followed by the samples obtained at a flow of 7.5 mL/h.

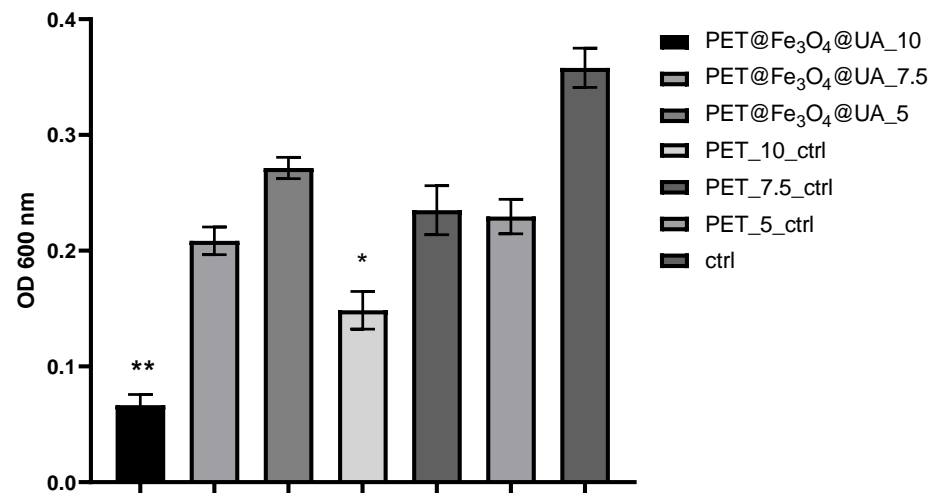


Figure 9. Graphical representation of the recorded absorbance values for *S. aureus* cultures, expressing the multiplication capacity of these cells after cultivation for 24 h in the presence of recycled PET polymer materials and control (planktonic microorganisms without materials). * $p < 0.05$; ** $p < 0.001$.

In the case of planktonic *P. aeruginosa* cultures, it was also observed that PET@Fe₃O₄@UA exhibited good inhibition against microbial development. Compared with the results observed for *S. aureus* cultures, *P. aeruginosa* growth inhibition is frequently lower in all experimental variants (Figure 10).

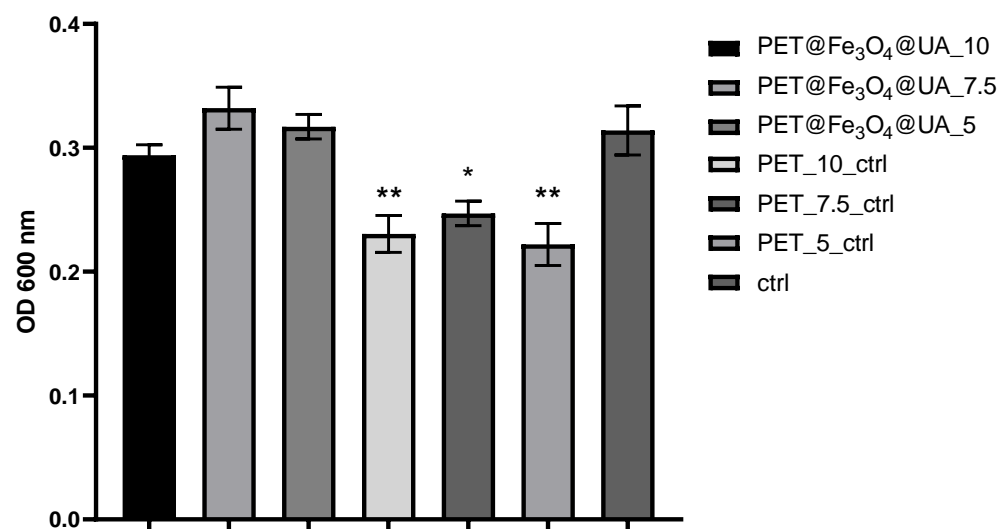


Figure 10. Graphical representation of the absorbance values recorded for *P. aeruginosa* cultures expressing the multiplication capacity of bacteria cells after cultivation for 24 h in the presence of recycled PET polymer materials and control (planktonic microorganisms without materials). * $p < 0.05$; ** $p < 0.001$.

In the case of the tested yeast strain, it can be observed that the effect of the obtained materials on the growth of planktonic *C. albicans* is relatively uniform for the samples obtained at a flow rate of 7.5 and 5 mL/h, which are similar to the control. However, growth is significantly inhibited by the sample obtained at a 10 mL/h flow rate (Figure 11).

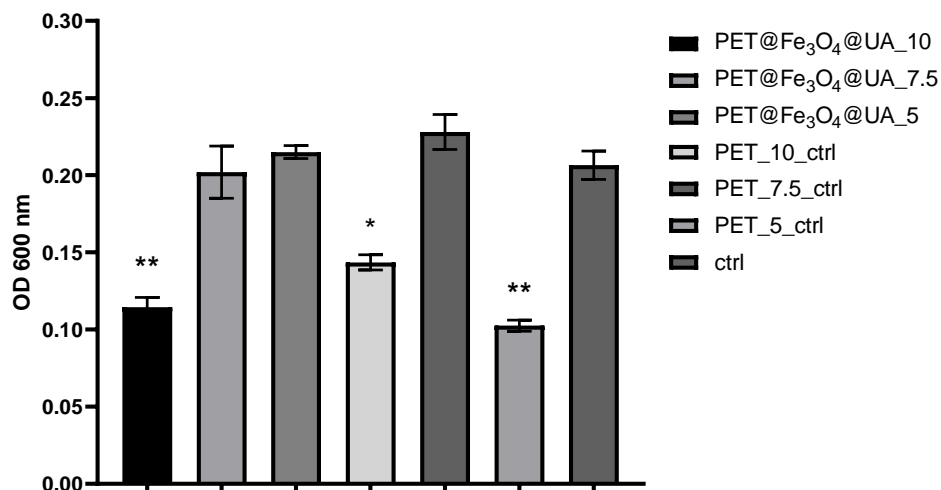


Figure 11. Graphical representation of the absorbance values recorded for cultures of *C. albicans*, expressing the multiplication capacity of these cells after cultivation for 24 h in the presence of recycled PET polymer materials and control (planktonic microorganisms without materials). * $p < 0.05$; ** $p < 0.001$.

The assessment of biofilm formation capacity proved different results than those obtained in planktonic cultures, suggesting that attachment inhibition and biofilm modulation may be a specific effect of these materials.

The inhibition effect of *S. aureus* biofilm development was achieved at all stages of biofilm development, starting with the cell adherence phase (up to 24 h), continuing with the maturation stage (up to 48 h) and until dispersion (when cells or cell aggregates detach from biofilm to colonize new surfaces) (Figure 12).

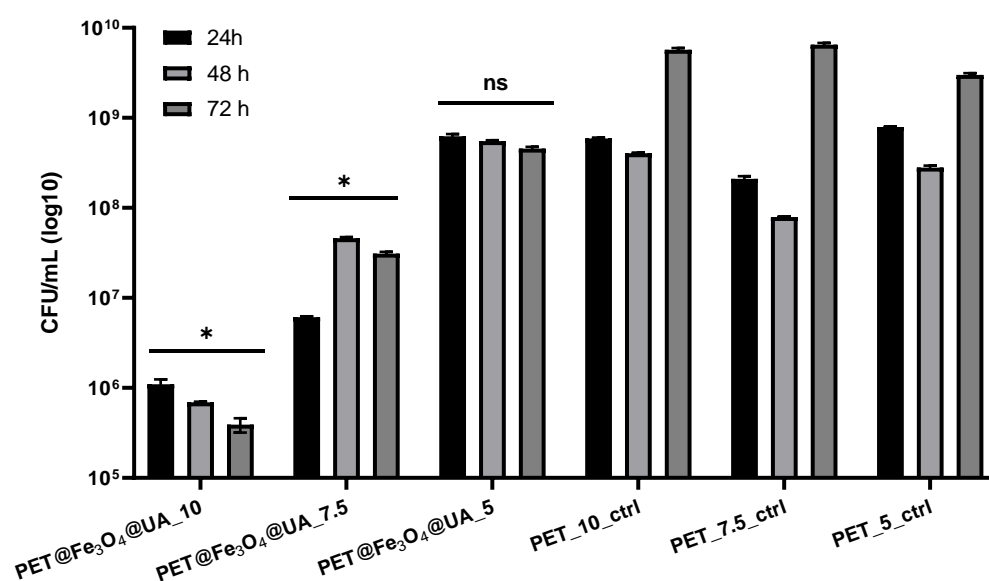


Figure 12. Graphical representation of CFU/mL (colony forming units/mL) representing the number of *S. aureus* cells included in the monospecific biofilms developed on the surface of the materials obtained for 24 h, 48 h, and 72 h at 37 °C. (* $p < 0.05$; by comparing biofilm formation on PET control and corresponding UA containing PET, ns = not significant).

PET@Fe₃O₄@UA has also demonstrated an effect of inhibiting the growth of biofilms produced by *S. aureus* at all time intervals analyzed, with the highest efficiency for the 5 mL/h samples.

P. aeruginosa is a bacterial species with various natural resistance mechanisms, being an opportunistic pathogen that can colonize and adhere efficiently in various environments. Biofilms produced by *P. aeruginosa* are difficult to eradicate with actual antimicrobial medicines [57]. The results presented in our study have shown that *P. aeruginosa* presents a limited ability to form biofilms onto the obtained nanostructured fibrous mats (Figure 13).

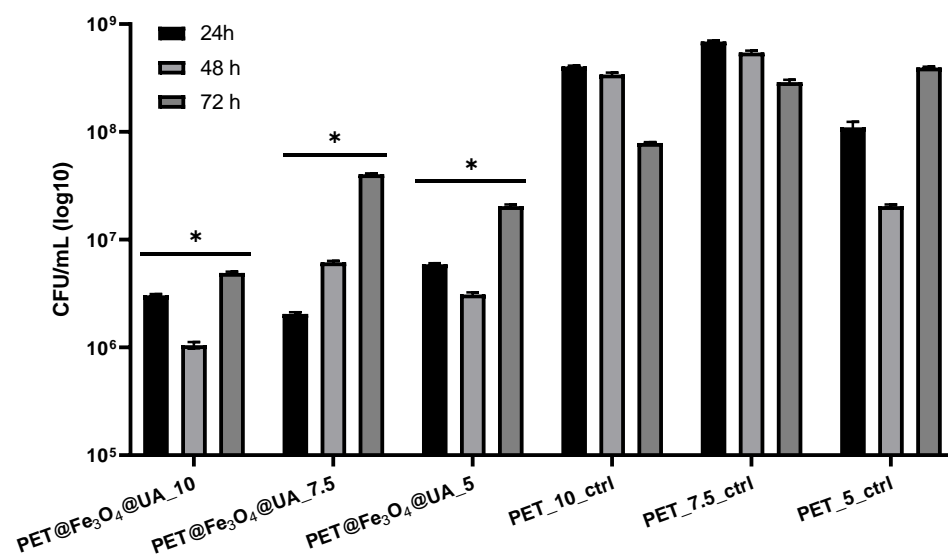


Figure 13. Graphical representation of CFU/mL (colony forming units/mL) representing the amount of *P. aeruginosa* cells included in the monospecific biofilms developed on the surface of the materials obtained for 24 h, 48 h, and 72 h at 37 °C. (* $p < 0.05$; by comparing biofilm formation on PET control and corresponding UA containing PET).

The obtained PET@Fe₃O₄@UA membranes produced significant inhibition of *P. aeruginosa* biofilms at all tested time intervals, regardless of the fiber flow rate deposition by electrospinning.

In the case of the *C. albicans* strain, significant biofilm development inhibition capacities can be observed in all experimental variants tested. All membranes based on PET and inorganic nanoparticles have shown an inhibitory effect on the development of *C. albicans* biofilms, regardless of the fiber deposition rate by electrospinning or the type of nano-system contained, and not being influenced by the action time (Figure 14).

While most studies focus on the antimicrobial effects of silver and gold nanoparticles, this study provides evidence of the efficiency of magnetite nanoparticles obtained onto the surface of PET nanofibers against microbial growth and colonization, still limited in the literature. The precise mechanisms involved could be associated with nanoparticles' properties in terms of reduced size and high surface-to-volume ratios, and surface reactivity [58].

Moreover, since the concentration of magnetite nanoparticles was not modified, the differences in the obtained samples' antimicrobial activity are influenced by the parameters applied in the electrospinning process. Precisely, the best results were obtained for the samples prepared with a feed rate of 10 mL/h in the case of *S. aureus* and *C. albicans*, both in planktonic and biofilm states. Reports from the available literature state that the feed rate parameter does not influence nanofibers' diameter [59,60]. As PET reported no intrinsic antimicrobial properties, the increased antimicrobial activity of the 10 mL/h samples could be associated with a higher number of magnetite nanoparticles formed onto the surface of the nanofibers.

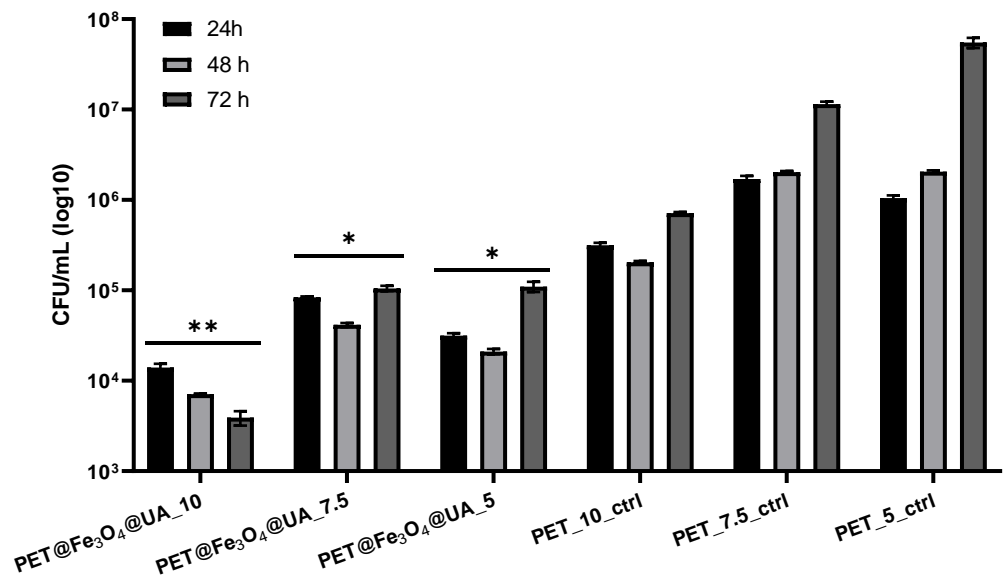


Figure 14. Graphic representation of CFU/mL (colony forming units/mL) representing the number of *C. albicans* cells included in the monospecific biofilms developed on the surface of the materials obtained for 24 h, 48 h, and 72 h at 37 °C. (* $p < 0.05$; ** $p < 0.001$ by comparing biofilm formation on PET control and corresponding UA containing PET).

Furthermore, results prove a higher efficiency of the obtained biomaterials against Gram-positive and yeast species than Gram-negative bacteria, possibly due to the differences in their structural features.

Figure 15 shows the effects of the subcutaneous implantation of PET@Fe₃O₄ on the serum level of the inflammatory marker CRP. At 24 h after implantation, serum CRP concentration increased for all experimental groups, followed by a 14-day decrease. The CRP level was decreased for PET@Fe₃O₄ implants compared to the PET control group.

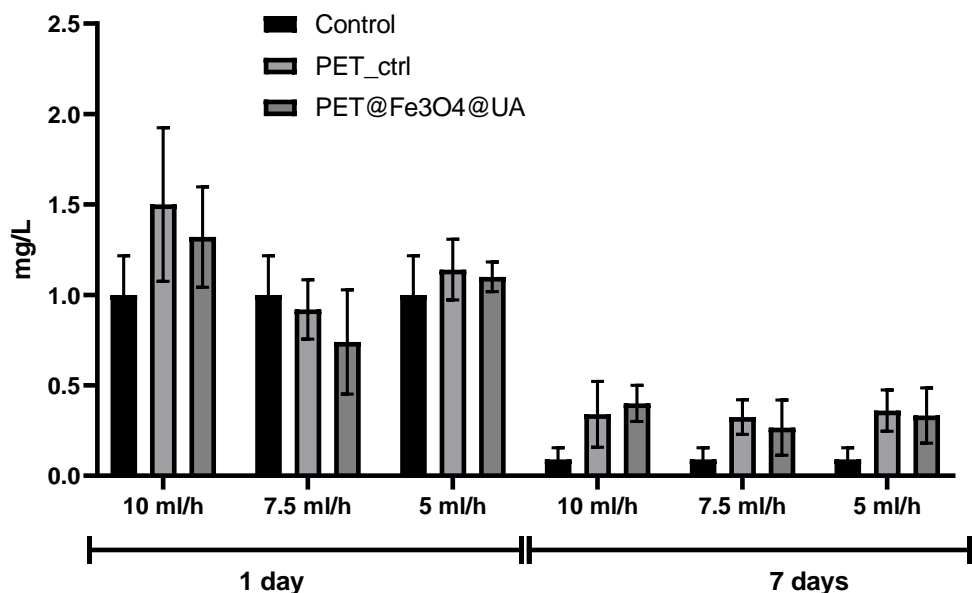


Figure 15. The effects of PET@Fe₃O₄@UA subcutaneous implantation in mice on the C-reactive protein (CRP) levels at 24 h and 7 days post-surgery.

The post-implantation clinical analysis revealed no local or systemic adverse effects. Histopathological analysis showed edema in the case of PET control at 24 h, which is maintained at 7 days after surgery (Figure 16). The inflammatory reaction is strongest for

PET control at 10 mL/h. The leukocyte count in the tissues surrounding these implants revealed the marked presence of PMN at 24 h, a sign of acute inflammation. At 7 days, they are replaced gradually with macrophages (Table 2). At this interval, the presence of fibroblasts and collagen deposits is noticed, highlighted by trichrome stain (Figure 16). The inflammatory reaction is much reduced in the case of PET coating with Fe₃O₄ nanoparticles functionalized with usnic acid, which decreased with the flow rate. Moreover, the repair process is highlighted, demonstrated by the newly formed capillaries in the damaged tissues around the implant (Table 2).

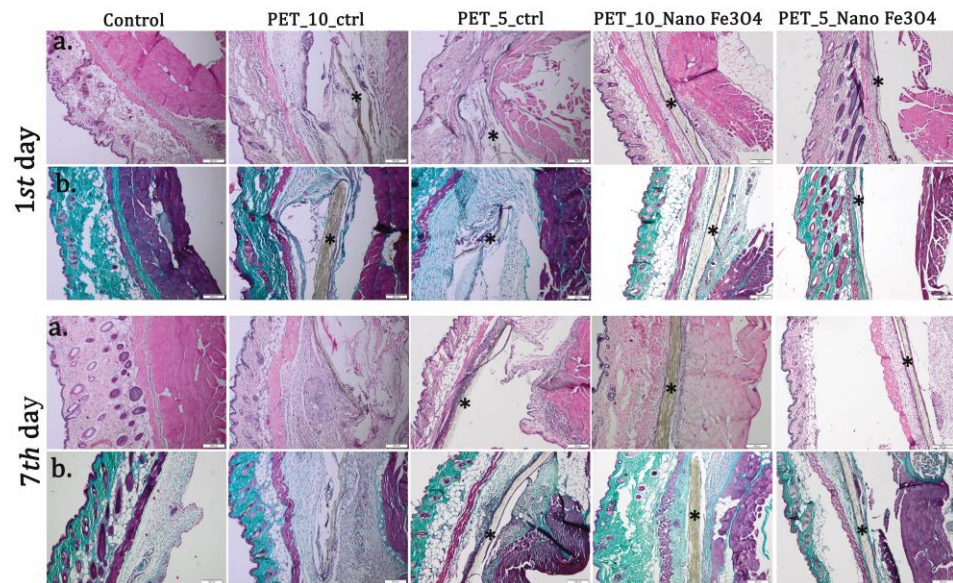


Figure 16. Biocompatibility analysis of PET_10_{ctrl}, PET_5_{ctrl}, PET_10_{Nano Fe₃O₄} and PET_5_{Nano Fe₃O₄} at 24 h and 7 days post-implantation. (a) H&E stain; (b) Masson-Goldner trichrome stain. Material (*); Scale bar 200 μ m.

Table 2. Histomorphometric scoring used to grade inflammation and neovascularization in the tissue surrounding subcutaneous implants.

Material	Implantation Period (Days)	Edema	PMN	M	F	NV
Control	1	—	+	—	—	—
	7	—	—	+	—	—
PET_10 _{ctrl}	1	++++	+++	++	+	—
	7	+++	++	+++	++++	—
PET_7.5 _{ctrl}	1	+++	+++	+	+	—
	7	++	+	+++	+++	—
PET_5 _{ctrl}	1	++	+++	+	+	—
	7	++	+	+++	++	+
PET@Fe ₃ O ₄ @UA ₁₀	1	+	++	+	+	—
	7	—	+	++	+++	++
PET@Fe ₃ O ₄ @UA _{7.5}	1	—	+	+	+	—
	7	—	—	++	++	++
PET@Fe ₃ O ₄ @UA ₅	1	—	+	—	+	—
	7	—	—	++	++	++

PMN: Polymorphonuclear neutrophils; M: Macrophages; F: Fibroblasts, NV: Neovascularization; Tissue reactions are rated from — (not present) until ++++ (extensive).

Immunofluorescence was performed for tissue sections to analyze inflammatory response towards the implanted materials. As shown in Figure 17, TNF- α immunostaining

increased on soft tissue surrounded by PET-materials with flow rate. The immunoreaction was decreased, though PET was coated with Fe_3O_4 .

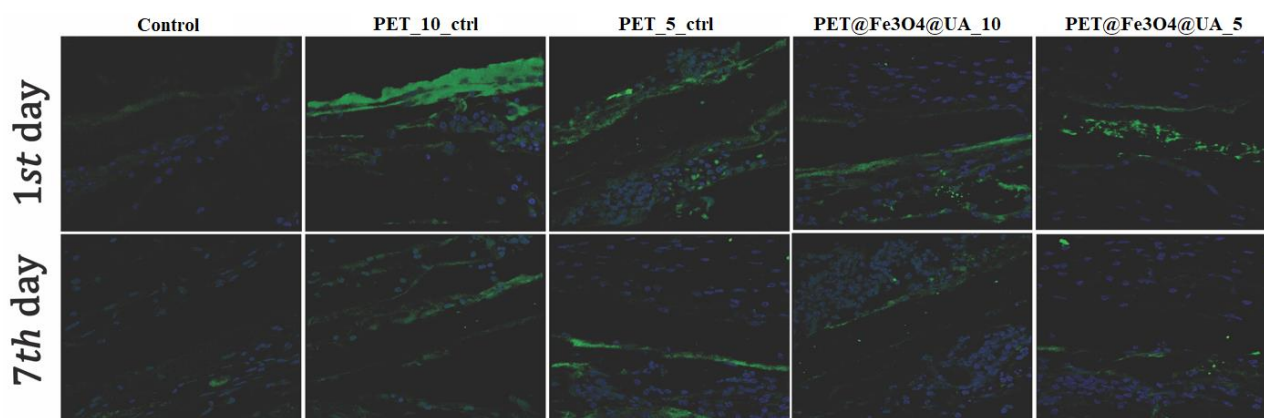


Figure 17. TNF- α protein expression as revealed by confocal microscopy at 24 h and 7 days post-implantation. TNF- α is labeled green, and the nuclei are counterstained with DAPI.

The rapid advancement of technology and nanoscience, along with the rapid dissemination of innovative findings, has allowed the development of nanofibers obtained via electrospinning. It is essential to note that this method differs from others because it allows for controlling of the diameter, morphology, orientation, and even fiber structure [61].

There are studies on the electrospinning of PET, but only a few published papers regarding the electrospinning of recycled PET, where electrospinning from melt was used to produce fibers in the nanometer–few micrometer range, with most applications in smoke or air filtration [61–63] or oil-water separation [64] and only a very small number concerning application in anti-infective therapy [39]. It is essential to keep in mind that the research into recycled materials has attracted an increased interest in the past decade, owing to the necessity to minimize waste and develop alternative sources of resources [61].

Voltage, ambient temperature, humidity, heat power, feed rate, and needle-to-target distance were all carried out thoroughly during the electrospinning process described in the present work. Optimal electrospinning conditions were achieved using a trial-and-error method at -5.73 kV, $+17.53$ kV, and 0.6 kW with different feed rates under ambient conditions of 35% relative humidity and a temperature of 27 °C. However, in the process of obtaining (nano)fibrous membrane using the ES technique, the voltage crucial because no fiber can be formed because the surface tension of the solution prevents the solution from flowing into the collector. A constant needle-to-target distance of 200 mm was maintained for all samples, given that the distance influences the fibers' diameter. To achieve that goal, one of the most important parameters of the electrospinning process was varied—rate deposition (feed rate— 5 mL/h, 7.5 mL/h, and 10 mL/h)—and their influence on fiber morphology, biocompatibility and antimicrobial and antibiofilm activity against Gram-positive and Gram-negative bacteria strains, but also on opportunistic yeast, was analyzed. The morphology of PET fibers was examined by scanning electron microscopy, Transmission Electron Microscopy, Fourier-Transform Infrared Spectroscopy, and X-ray Diffraction. A nanostructured fibrous mat with diameters ranging from 50 to 150 nm is noticed for all experimental feed rates according to SEM images. Moreover, we can establish that $\text{Fe}_3\text{O}_4@UA$ are randomly distributed on the samples, frequently at the junction of the fibers, which are considered as nucleation centers promoting the growth of magnetite nanocrystals. Besides, the particle size observed on the surface of the junction between the fibers ranges from 5 to 10 nm. These results were also confirmed by Transmission Electron Microscopy. Moreover, these fibrillar nanoparticle-containing membranes showed good inhibition in vitro due to usnic acid-functionalized magnetic nanoparticles presenting a remarkably enhanced antimicrobial activity against both Gram-positive (*S. aureus*) and Gram-negative (*P. aeruginosa*) bacteria strains, but also on opportunistic yeast *C. albicans*, as

compared to control. The functionalized fibrous mat also showed low toxicity *in vivo*, and clinical analysis performed post-implantation revealed no local or systemic adverse effects.

Thus, the findings presented in this study open up new possibilities for PET recycling, such as combining it with other antimicrobial inorganic nanostructures to create enhanced fibrillar materials with antimicrobial and antibiofilm capabilities. Such technologies could be used in the food business, particularly for food packing, as well as in the biomedical field, to generate antimicrobial medical fabrics.

4. Conclusions

The obtained PET nanostructured membranes showed an improved antimicrobial and antibiofilm activity against model Gram-positive (*S. aureus*) and Gram-negative (*P. aeruginosa*) bacteria strains, but also on opportunistic yeast *C. albicans*. The best results in terms of antimicrobial potential were obtained for the samples obtained at higher feed rates due to the formation of denser meshes and with higher amounts of magnetite nanoparticles on their surface (qualitative observation). Moreover, these fibrillar nanoparticle-containing membranes showed low toxicity *in vitro* and *in vivo*. The results open new perspectives for PET recycling, such as its use combined with various antimicrobial inorganic nanostructures to obtain improved fibrillar materials with antimicrobial and antibiofilm properties. Such systems could be further utilized in the food industry, especially for food packaging applications, but also in the biomedical field to develop antimicrobial medical textiles.

Author Contributions: Conceptualization and designed the experiments, A.M.G., E.A., A.O.H. and A.E.S.; methodology, A.M.G., A.O.H. and A.M.H.; validation, A.M.G. and E.A.; synthesis, A.E.S., formal analysis, B.S.V., A.M.H., H.H., B.C., M.R., A.F. and S.G.; D.E.M.; investigation, A.E.S., A.C.B., A.M.G., B.S.V., A.M.H., H.H., B.C., A.O.H., M.R., S.G., A.F. and D.E.M.; writing—original draft preparation, A.E.S., A.C.B.; writing—review and editing, A.E.S. and A.M.G.; supervision, A.O.H. and A.M.G. All authors have read and agreed to the published version of the manuscript.

Funding: This work was supported by the grant POCU/993/6/13-153178, co-financed by the European Social Fund within the Sectorial Operational Program Human Capital 2014–2020 and Romanian Governmental through the National Programme “Installations and Strategic Objectives of National Interest”. The FT-ICR-MS analyses were possible due to European Regional Development Fund through Competitiveness Operational Program 2014–2020, Priority Axis 1, Project No. P_36_611, MySMIS code 107066, INOVABIOMED.

Institutional Review Board Statement: Declared none.

Data Availability Statement: Available at the authors, at request.

Acknowledgments: This work was supported by the grant POCU/993/6/13 -153178, co-financed by the European Social Fund within the Sectorial Operational Program Human Capital 2014–2020 and Romanian Governmental through the National Programme “Installations and Strategic Objectives of National Interest”. The FT-ICR-MS analyses were possible due to European Regional Development Fund through Competitiveness Operational Program 2014–2020, Priority Axis 1, Project No. P_36_611, MySMIS code 107066, INOVABIOMED.

Conflicts of Interest: The authors declare no conflict of interest.

References

1. Prakash, P.; Sowmya, N.; Sudha, S.; Masilamani Selvam, M.; Pully, D.; Shobana, N.; Saigeetha, S.; Samrot, A.V. Isolation and Characterization of Chitin Nanofibers from *Calocybe indica* and its Applications. *Letts. Appl. NanoBioScience* **2022**, *11*, 4105–4113. [[CrossRef](#)]
2. Daels, N.; De Vrieze, S.; Sampers, I.; Decostere, B.; Westbroek, P.; Dumoulin, A.; Dejans, P.; De Clerck, K.; Van Hulle, S. Potential of a functionalised nanofibre microfiltration membrane as an antibacterial water filter. *Desalination* **2011**, *275*, 285–290. [[CrossRef](#)]
3. Ki, C.S.; Kim, J.W.; Hyun, J.H.; Lee, K.H.; Hattori, M.; Rah, D.K.; Park, Y.H. Electrospun three-dimensional silk fibroin nanofibrous scaffold. *J. Appl. Polym. Sci.* **2007**, *106*, 3922–3928. [[CrossRef](#)]
4. Afrash, H.; Nazeri, N.; Davoudi, P.; FaridiMajidi, R.; Ghanbari, H. Development of a Bioactive Scaffold based on NGF Containing PCL/Chitosan Nanofibers for Nerve Regeneration. *Biointerface Res. Appl. Chem.* **2021**, *11*, 12606–12617. [[CrossRef](#)]
5. Huang, J.; Liu, Y.; You, T. Carbon nanofiber based electrochemical biosensors: A review. *Anal. Methods* **2010**, *2*, 202–211. [[CrossRef](#)]

6. Fathi, S.; Saber, R.; Adabi, M.; Rasouli, R.; Douraghi, M.; Morshedi, M.; Farid-Majidi, R. Novel Competitive Voltam metric Aptasensor Based on Electrospun Carbon Nanofibers-Gold Nanoparticles Modified Graphite Electrode for Salmonella enterica serovar Detection. *Biointerface Res. Appl. Chem.* **2021**, *11*, 8702–8715. [[CrossRef](#)]
7. Khil, M.S.; Cha, D.I.; Kim, H.Y.; Kim, I.S.; Bhattarai, N. Electrospun nanofibrous polyurethane membrane as wound dressing. *J. Biomed. Mater. Res. Part B Appl. Biomater.* **2003**, *67*, 675–679. [[CrossRef](#)] [[PubMed](#)]
8. Ketabchi, N.; Dinarvand, R.; Adabi, M.; Gholami, M.; Firoozi, S.; Amanzadi, B.; Faridi-Majidi, R. Study of Third-Degree Burn Wounds Debridement and Treatment by Actinidin Enzyme Immobilized on Electrospun Chitosan/PEO Nanofibers in Rats. *Biointerface Res. Appl. Chem.* **2021**, *11*, 10358–10370. [[CrossRef](#)]
9. Wang, C.; Li, Y.; Ding, G.; Xie, X.; Jiang, M. Preparation and characterization of graphene oxide/poly (vinyl alcohol) composite nanofibers via electrospinning. *J. Appl. Polym. Sci.* **2013**, *127*, 3026–3032. [[CrossRef](#)]
10. Güler, B. Comparative analysis of superabsorbent properties of PVP and PAA nanofibres. *Ind. Textila* **2021**, *72*, 460–466. [[CrossRef](#)]
11. Gorji, M.; Jeddi, A.; Gharehaghaji, A. Fabrication and characterization of polyurethane electrospun nanofiber membranes for protective clothing applications. *J. Appl. Polym. Sci.* **2012**, *125*, 4135–4141. [[CrossRef](#)]
12. Yoo, H.S.; Kim, T.G.; Park, T.G. Surface-functionalized electrospun nanofibers for tissue engineering and drug delivery. *Adv. Drug Deliv. Rev.* **2009**, *61*, 1033–1042. [[CrossRef](#)] [[PubMed](#)]
13. Kamaci, U.D.; Peksel, A. Poly(vinyl alcohol)-based Electrospun Nanofibers: Characterization and Phytase Immobilization. *Biointerface Res. Appl. Chem.* **2022**, *12*, 7573–7583. [[CrossRef](#)]
14. Alghoraibi, I.; Alomari, S. Different Methods for Nanofiber Design and Fabrication. In *Handbook of Nanofibers*; Barhoum, A., Bechelany, M., Makhlof, A., Eds.; Springer International Publishing: Cham, Switzerland, 2018; pp. 1–46.
15. Lu, P.; Ding, B. Applications of electrospun fibers. *Recent Pat. Nanotechnol.* **2008**, *2*, 169–182. [[CrossRef](#)]
16. Sivri, Ç.; Haji, A. Nanofiber production from rose water and mate plant extract solutions using environmentally friendly electrospinning. *Ind. Textila* **2022**, *73*, 595–601. [[CrossRef](#)]
17. Huang, Z.-M.; Zhang, Y.-Z.; Kotaki, M.; Ramakrishna, S. A review on polymer nanofibers by electrospinning and their applications in nanocomposites. *Compos. Sci. Technol.* **2003**, *63*, 2223–2253. [[CrossRef](#)]
18. Anbalagan, S.; Venkatakrishnan, H.R.R.; Ravindran, J.; Sathyamoorthy, J.; Rangabashyam, K.A.; Ragini, Y.P.; Sathasivam, J. Hydrolytic Degradation of Polyethylene Terephthalate by Cutinase Enzyme Derived from Fungal Biomass-Molecular Characterization. *Biointerface Res. Appl. Chem.* **2022**, *12*, 653–667. [[CrossRef](#)]
19. Yang, M.-R.; Chen, K.-S.; Tsai, J.-C.; Tseng, C.-C.; Lin, S.-F. The antibacterial activities of hydrophilic-modified nonwoven PET. *Mater. Sci. Eng. C* **2002**, *20*, 167–173. [[CrossRef](#)]
20. Wang, J.; Huang, N.; Yang, P.; Leng, Y.; Sun, H.; Liu, Z.; Chu, P. The effects of amorphous carbon films deposited on polyethylene terephthalate on bacterial adhesion. *Biomaterials* **2004**, *25*, 3163–3170. [[CrossRef](#)] [[PubMed](#)]
21. Nisticò, R. Polyethylene terephthalate (PET) in the packaging industry. *Polym. Test.* **2020**, *90*, 106707. [[CrossRef](#)]
22. Naveed, T.; Babar, A.A.; Ramzan, B.M.; Naeem, A.M.; Awais, M.; Anwar, F.; Fraz, A.; Abbas, M. Influence of rotor structure and process parameters on polyethylene oxide (PEO) nanofibers produced through centrifugal. *Ind. Textila* **2022**, *73*, 479–491. [[CrossRef](#)]
23. Mansour, S.; Ikladious, N. Depolymerization of poly (ethylene terephthalate) waste using 1, 4-butanediol and triethylene glycol. *J. Elastomers Plast.* **2003**, *35*, 133–148. [[CrossRef](#)]
24. Samak, N.A.; Jia, Y.; Sharshar, M.M.; Mu, T.; Yang, M.; Peh, S.; Xing, J. Recent advances in biocatalysts engineering for polyethylene terephthalate plastic waste green recycling. *Environ. Int.* **2020**, *145*, 106144. [[CrossRef](#)] [[PubMed](#)]
25. Kamalakannan, S.; Kovendan, K.; Balachandar, V.; Naik, K.G.; Chauhan, A. Sources of Potential Fungi Generated Biogenic Nanoparticles for the Control of Diseases Transmitting Mosquitoes: A Review. *Lett. Appl. NanoBioScience* **2022**, *11*, 3523–3536. [[CrossRef](#)]
26. Habtemariam, A.B. Biosynthesis of Magnetite (Fe₃O₄) Nanostructures using Vernonia Amygdalina Leaves Extract. *Lett. Appl. NanoBioScience* **2021**, *10*, 2777–2783. [[CrossRef](#)]
27. Kim, Y.S.; Kim, Y.H. Application of ferro-cobalt magnetic fluid for oil sealing. *J. Magn. Magn. Mater.* **2003**, *267*, 105–110. [[CrossRef](#)]
28. Zarei, S.; Sadighian, S.; Rostamizadeh, K.; Khalkhali, M. Theragnostic Magnetic Core-Shell Nanoparticle as Versatile Nanoplatfor for Magnetic Resonance Imaging and Drug Delivery. *Biointerface Res. Appl. Chem.* **2021**, *11*, 13276–13289. [[CrossRef](#)]
29. Shen, L.; Laibinis, P.E.; Hatton, T.A. Bilayer surfactant stabilized magnetic fluids: Synthesis and interactions at interfaces. *Langmuir* **1999**, *15*, 447–453. [[CrossRef](#)]
30. Abbasi, S. Magnetic Particles Weight as an Indicator for Heavy Metals Concentration. *Lett. Appl. NanoBioScience* **2022**, *11*, 3770–3779. [[CrossRef](#)]
31. Cao, J.; Wang, Y.; Yu, J.; Xia, J.; Zhang, C.; Yin, D.; Häfeli, U.O. Preparation and radiolabeling of surface-modified magnetic nanoparticles with rhenium-188 for magnetic targeted radiotherapy. *J. Magn. Magn. Mater.* **2004**, *277*, 165–174. [[CrossRef](#)]
32. Jordan, A.; Scholz, R.; Wust, P.; Fähling, H.; Felix, R. Magnetic fluid hyperthermia (MFH): Cancer treatment with AC magnetic field induced excitation of biocompatible superparamagnetic nanoparticles. *J. Magn. Magn. Mater.* **1999**, *201*, 413–419. [[CrossRef](#)]
33. Zhang, M.; Song, W.; Tang, Y.; Xu, X.; Huang, Y.; Yu, D. Polymer-based nanofiber–nanoparticle hybrids and their medical applications. *Polymers* **2022**, *14*, 351. [[CrossRef](#)] [[PubMed](#)]

34. Jordan, A.; Scholz, R.; Wust, P.; Schirra, H.; Schiestel, T.; Schmidt, H.; Felix, R. Endocytosis of dextran and silan-coated magnetite nanoparticles and the effect of intracellular hyperthermia on human mammary carcinoma cells in vitro. *J. Magn. Magn. Mater.* **1999**, *194*, 185–196. [[CrossRef](#)]
35. Wei, Y.; Han, B.; Hu, X.; Lin, Y.; Wang, X.; Deng, X. Synthesis of Fe₃O₄ nanoparticles and their magnetic properties. *Procedia Eng.* **2012**, *27*, 632–637. [[CrossRef](#)]
36. Sadighian, S.; Sharifan, K.; Khanmohammadi, A.; Rohani, M.K. A Facile Synthesis of Fe₃O₄@SiO₂@ZnO for Curcumin Delivery. *Biointerface Res. Appl. Chem.* **2022**, *12*, 7994–8002. [[CrossRef](#)]
37. Rodrigues, G.R.; López-Abarrategui, C.; de la Serna Gómez, I.; Dias, S.C.; Otero-González, A.J.; Franco, O.L. Antimicrobial magnetic nanoparticles based-therapies for controlling infectious diseases. *Int. J. Pharm.* **2019**, *555*, 356–367. [[CrossRef](#)] [[PubMed](#)]
38. Medina-Cruz, D.; Saleh, B.; Vernet-Crua, A.; Ajo, A.; Roy, A.K.; Webster, T.J. Chapter 22—Drug-delivery nanocarriers for skin wound-healing applications. In *Wound Healing, Tissue Repair, and Regeneration in Diabetes*; Bagchi, D., Das, A., Roy, S., Eds.; Academic Press: New York, NY, USA, 2020; pp. 439–488.
39. Grumezescu, A.M.; Stoica, A.E.; Dima-Bălcescu, M.-Ş.; Chircov, C.; Gharbia, S.; Baltă, C.; Roşu, M.; Herman, H.; Holban, A.M.; Ficai, A.; et al. Electrospun Polyethylene Terephthalate Nanofibers Loaded with Silver Nanoparticles: Novel Approach in Anti-Infective Therapy. *J. Clin. Med.* **2019**, *8*, 1039. [[CrossRef](#)]
40. Grumezescu, A.; Vasile, B.; Holban, A. Eugenol functionalized magnetite nanostructures used in anti-infectious therapy. *Lett. Appl. Nanobiosci.* **2013**, *2*, 120–123.
41. Grumezescu, A.M.; Cotar, A.I.; Andronescu, E.; Ficai, A.; Ghitulica, C.D.; Grumezescu, V.; Vasile, B.S.; Chifiriuc, M.C. In vitro activity of the new water-dispersible Fe₃O₄@ usnic acid nanostructure against planktonic and sessile bacterial cells. *J. Nanoparticle Res.* **2013**, *15*, 035002. [[CrossRef](#)]
42. Anghel, A.G.; Grumezescu, A.M.; Chirea, M.; Grumezescu, V.; Socol, G.; Iordache, F.; Oprea, A.E.; Anghel, I.; Holban, A.M. MAPLE Fabricated Fe₃O₄@Cinnamomum verum Antimicrobial Surfaces for Improved Gastrostomy Tubes. *Molecules* **2014**, *19*, 8981–8994. [[CrossRef](#)]
43. Ahn, B.W.; Kang, T.J. Preparation and characterization of magnetic nanofibers with iron oxide nanoparticles and poly(ethylene terephthalate). *Mater. Sci.* **2012**, *125*, 1567–1575. [[CrossRef](#)]
44. Sung, Y.K.; Ahn, B.W.; Kang, T.J. Magnetic nanofibers with core (Fe₃O₄ nanoparticle suspension)/sheath (poly ethylene terephthalate) structure fabricated by coaxial electrospinning. *J. Magn. Magn. Mater.* **2012**, *324*, 916–922. [[CrossRef](#)]
45. Rădulescu, M.; Andronescu, E.; Holban, A.M.; Vasile, B.S.; Iordache, F.; Mogoantă, L.; Mogoşanu, G.D.; Grumezescu, A.M.; Georgescu, M.; Chifiriuc, M.C. Antimicrobial Nanostructured Bioactive Coating Based on Fe₃O₄ and Patchouli Oil for Wound Dressing. *Metals* **2016**, *6*, 103. [[CrossRef](#)]
46. Chen, R.; Cheng, J.; Wei, Y. Preparation and magnetic properties of Fe₃O₄ microparticles with adjustable size and morphology. *J. Alloys Compd.* **2012**, *520*, 266–271. [[CrossRef](#)]
47. Bortolassi, A.C.C.; Nagarajan, S.; de Araújo Lima, B.; Guerra, V.G.; Aguiar, M.L.; Huon, V.; Soussan, L.; Cornu, D.; Miele, P.; Bechelany, M. Efficient nanoparticles removal and bactericidal action of electrospun nanofibers membranes for air filtration. *Mater. Sci. Eng. C* **2019**, *102*, 718–729. [[CrossRef](#)] [[PubMed](#)]
48. Lala, N.L.; Ramaseshan, R.; Bojun, L.; Sundarrajan, S.; Barhate, R.S.; Ying-jun, L.; Ramakrishna, S. Fabrication of nanofibers with antimicrobial functionality used as filters: Protection against bacterial contaminants. *Biotechnol. Bioeng.* **2007**, *97*, 1357–1365. [[CrossRef](#)] [[PubMed](#)]
49. Abbas, J.A.; Said, I.A.; Mohamed, M.A.; Yasin, S.A.; Ali, Z.A.; Ahmed, I.H. Electrospinning of polyethylene terephthalate (PET) nanofibers: Optimization study using taguchi design of experiment. *IOP Conf. Ser. Mater. Sci. Eng.* **2018**, *454*, 012130. [[CrossRef](#)]
50. Ma, Z.; Kotaki, M.; Yong, T.; He, W.; Ramakrishna, S. Surface engineering of electrospun polyethylene terephthalate (PET) nanofibers towards development of a new material for blood vessel engineering. *Biomaterials* **2005**, *26*, 2527–2536. [[CrossRef](#)]
51. El-Saftawy, A.A.; Elfalaky, A.; Ragheb, M.S.; Zakhary, S.G. Electron beam induced surface modifications of PET film. *Radiat. Phys. Chem.* **2014**, *102*, 96–102. [[CrossRef](#)]
52. Khairiah, B.; Lily, I.M.D.; Nur, A.A.A.J.S.M. Rigid Polyurethane Foam from Glyco lysed Polyethylene Terephthalate Dissolved in Palm-based Polyol. *Sains Malays.* **2013**, *42*, 449–457.
53. Paszkiewicz, S.; Szymczyk, A.; Pawlikowska, D.; Irska, I.; Taraghi, I.; Pilawka, R.; Gu, J.; Li, X.; Tu, Y.; Piesowicz, E. Synthesis and characterization of poly(ethylene terephthalate-co-1,4-cyclohexanedimethylene terephthalate)-block-poly(tetramethylene oxide) copolymers. *RSC Adv.* **2017**, *7*, 41745–41754. [[CrossRef](#)]
54. Peltzer, M.A.; Simoneau, C. *Report of an Interlaboratory Comparison from the European Reference Laboratory for Food Contact Materials*; Publications Office of the European Union: Luxembourg, 2013.
55. Stewart, P.S. Antimicrobial Tolerance in Biofilms. *Microbiol. Spectr.* **2015**, *3*. [[CrossRef](#)] [[PubMed](#)]
56. Curutiu, C.; Ditu, L.M.; Iordache, F.; Bleotu, C.; Chifiriuc, M.C.; Lazar, V.; Paduraru, D.N.; Holban, A.M.J.B.R.I.A.C. Quorum Sensing molecules produced by *Pseudomonas aeruginosa* impair attachment and biofilm formation in *Candida albicans*. *Biointerface Res. Appl. Chem.* **2017**, *7*, 2016–2020.
57. Furiga, A.; Lajoie, B.; El Hage, S.; Baziard, G.; Roques, C. Impairment of *Pseudomonas aeruginosa* biofilm resistance to antibiotics by combining the drugs with a new quorum-sensing inhibitor. *Antimicrob. Agents Chemother.* **2016**, *60*, 1676–1686. [[CrossRef](#)] [[PubMed](#)]

58. Arakha, M.; Pal, S.; Samantarrai, D.; Panigrahi, T.K.; Mallick, B.C.; Pramanik, K.; Mallick, B.; Jha, S. Antimicrobial activity of iron oxide nanoparticle upon modulation of nanoparticle-bacteria interface. *Sci. Rep.* **2015**, *5*, 14813. [[CrossRef](#)]
59. Fallahi, D.; Rafizadeh, M.; Mohammadi, N.; Vahidi, B. Effects of feed rate and solution conductivity on jet current and fiber diameter in electrospinning of polyacrylonitrile solutions. *J. E-Polymers* **2009**, *9*, 250. [[CrossRef](#)]
60. Zhu, G.; Zhao, L.Y.; Zhu, L.T.; Deng, X.Y.; Chen, W.L. Effect of Experimental Parameters on Nanofiber Diameter from Electrospinning with Wire Electrodes. *IOP Conf. Ser. Mater. Sci. Eng.* **2017**, *230*, 012043. [[CrossRef](#)]
61. Bonfim, D.P.F.; Cruz, F.G.S.; Guerra, V.G.; Aguiar, M.L. Development of Filter Media by Electrospinning for Air Filtration of Nanoparticles from PET Bottles. *Membranes* **2021**, *11*, 293. [[CrossRef](#)]
62. Strain, I.; Wu, Q.; Pourrahimi, A.M.; Hedenqvist, M.S.; Olsson, R.T.; Andersson, R.L. Electrospinning of recycled PET to generate tough mesomorphic fibre membranes for smoke filtration. *J. Mater. Chem. A* **2015**, *3*, 1632–1640. [[CrossRef](#)]
63. Hossain, M.T.; Shahid, M.A.; Ali, A. Development of nanofibrous membrane from recycled polyethylene terephthalate bottle by electrospinning. *OpenNano* **2022**, *8*, 100089. [[CrossRef](#)]
64. Doan, H.N.; Phong Vo, P.; Hayashi, K.; Kinashi, K.; Sakai, W.; Tsutsumi, N. Recycled PET as a PDMS-Functionalized electrospun fibrous membrane for oil-water separation. *J. Environ. Chem. Eng.* **2020**, *8*, 103921. [[CrossRef](#)]

Disclaimer/Publisher's Note: The statements, opinions and data contained in all publications are solely those of the individual author(s) and contributor(s) and not of MDPI and/or the editor(s). MDPI and/or the editor(s) disclaim responsibility for any injury to people or property resulting from any ideas, methods, instructions or products referred to in the content.